

# Dependence of Halo Bias and Kinematics on Assembly Variables

Xiaoju Xu<sup>★</sup> and Zheng Zheng<sup>†</sup>

*Department of Physics and Astronomy, University of Utah, 115 South 1400 East, Salt Lake City, UT 84112, USA*

Accepted XXX. Received YYY; in original form ZZZ

## ABSTRACT

Using dark matter haloes identified in a large  $N$ -body simulation, we study halo assembly bias, with halo formation time, peak maximum circular velocity, concentration, and spin as the assembly variables. Instead of grouping haloes at fixed mass into different percentiles of each assembly variable, we present the joint dependence of halo bias on the *values* of halo mass and each assembly variable. In the plane of halo mass and one assembly variable, the joint dependence can be largely described as halo bias increasing outward from a global minimum. We find it unlikely to have a combination of halo variables to absorb all assembly bias effects. We then present the joint dependence of halo bias on two assembly variables at fixed halo mass. The gradient of halo bias does not necessarily follow the correlation direction of the two assembly variables and it varies with halo mass. Therefore in general for two correlated assembly variables one cannot be used as a proxy for the other in predicting halo assembly bias trend. Finally, halo assembly is found to affect the kinematics of haloes. Low-mass haloes formed earlier can have much higher pairwise velocity dispersion than those of massive haloes. In general, halo assembly leads to a correlation between halo bias and halo pairwise velocity distribution, with more strongly clustered haloes having higher pairwise velocity and velocity dispersion. However, the correlation is not tight, and the kinematics of haloes at fixed halo bias still depends on halo mass and assembly variables.

**Key words:** galaxies: haloes – galaxies: statistics – cosmology: theory – large-scale structure of Universe

## 1 INTRODUCTION

Large-volume galaxy redshift surveys over a range of redshifts, including the Sloan Digital Sky Survey (SDSS; York et al. 2000), the Two-degree Field Galaxy Redshift Survey (2dFGRS; Colless 1999), the SDSS-III (Eisenstein et al. 2011) and SDSS-IV (Dawson et al. 2016), and the WiggleZ Dark Energy Survey (Blake et al. 2011), have transformed the study of large-scale structure, producing detailed distribution of galaxies in the universe as a function of their properties and resulting in galaxy clustering measurements with high precision. Galaxy clustering data from such surveys play an important role in understanding galaxy formation and evolution and in learning about cosmology, in particular in constraining dark energy and testing gravitational theories.

The formation of galaxies involves poorly understood baryonic processes, causing a hurdle to interpret galaxy clustering data. In contrast, the formation and evolution of dark matter haloes are dominated by gravitational interactions and their properties are well understood with analytic models and  $N$ -body simulations (e.g. Press & Schechter 1974; Mo & White 1996; Tinker et al. 2008). Over the past two decades, an informative way to interpret galaxy clustering has been developed and made wide applications, which is to link galaxies to the underlying dark matter halo population. The two commonly adopted descriptions of the galaxy-halo connection are the halo occupation distribution (HOD) and conditional luminosity function (CLF) frameworks (e.g. Berlind & Weinberg 2002; Yang et al. 2003; Zheng et al. 2005), which have been successfully applied to galaxy clustering data to infer the relation between galaxy properties and halo mass (e.g. Zehavi et al. 2005, 2011).

The HOD/CLF framework chooses the halo mass as the halo variable, and the implicit assumption is that

<sup>★</sup> E-mail: xiaoju.xu@utah.edu

<sup>†</sup> E-mail: zhengzheng@astro.utah.edu

the statistical properties of galaxies inside haloes only depend on halo mass, not on halo environment or growth history. This assumption of an environment-independent HOD/CLF is partly motivated by the excursion set theory (Bond et al. 1991). However,  $N$ -body simulations show that the clustering of haloes depends on not only halo mass, but also halo assembly history (e.g. Gao et al. 2005; Zhu et al. 2006; Jing et al. 2007), halo structure (e.g. Wechsler et al. 2006; Gao & White 2007; Faltenbacher & White 2010; Paranjape & Padmanabhan 2017), and halo environment (e.g. Harker et al. 2006; Salcedo et al. 2018), which is termed as *halo assembly bias*. Halo properties that correlate with halo environment or assembly history are broadly referred to here as halo assembly variables, such as halo formation time, halo concentration, maximum circular velocity of halo, and halo spin. Studying the origin of halo assembly bias remains active ongoing effort (e.g. Borzyszkowski et al. 2017). For massive haloes (with mass higher than the non-linear mass  $M_{\text{nl}}$  for collapse), the assembly bias appears to be a generic feature in the Extended Press-Schechter theory, related to the difference in the curvature of peaks of the same height in a Gaussian density field (e.g. Dalal et al. 2008). For low mass haloes, the assembly bias is proposed to be originated from the strong influence of the environment, especially the tidal field, on the evolution of haloes (e.g. Hahn et al. 2007, 2009; Wang et al. 2011; Shi et al. 2015).

Whether halo assembly bias is inherited by galaxies is still under investigation in both simulations (e.g. Chaves-Montero et al. 2016; Busch & White 2017; Garaldi et al. 2018) and observations (e.g. Lin et al. 2016; Miyatake et al. 2016; Guo et al. 2017; Zu et al. 2017). If galaxy properties are closely tied to halo growth history, the inherited assembly bias from the host haloes would require a modification of the current halo model of galaxy clustering to include such an effect. Otherwise, we would infer incorrect galaxy-halo connections and introduce possible systematics in cosmological constraints (e.g. Zentner et al. 2014; Hearin 2015; Zentner et al. 2016; but see McEwen & Weinberg 2016). Along the path, a better characterisation of halo assembly bias is necessary, which motivates the work in this paper. In most previous studies, halo assembly bias is inferred by grouping each halo assembly variable at fixed halo mass into certain percentiles. While this can reveal the trend of assembly bias, it does not provide a clear view on the multivariate dependence of the halo bias, which needs the measurement of halo bias at certain values, not certain percentiles, of a given assembly variable. If halo assembly effect is to be incorporated into the halo modelling of galaxy clustering, a natural route is to describe halo bias in terms of multiple halo properties. We will present the multivariate dependence of halo bias and study whether there is a combination of halo variables to minimise assembly bias. In addition, we also investigate the scale dependence of halo assembly bias and the assembly effect on halo kinematics.

The structure of the paper is as follows. In Section 2, we describe the simulation data used in this study and the measurement of halo bias. In Section 3, we present the joint dependence of halo bias on halo mass and each halo assembly variable, study an effective halo variable to minimise halo assembly bias, show the scale dependence of halo assembly bias, and describe the dependence of halo bias on two halo assembly variables. In Section 4, we analyse the assembly

effect on halo kinematics. Finally, in Section 5, we summarise our results and discuss their implications.

## 2 SIMULATION AND HALO BIAS CALCULATION

For the work presented in this paper, we make use of the MDR1 MultiDark simulation (Prada et al. 2012; ?)<sup>1</sup>. The MDR1  $N$ -body simulation adopts a spatially flat  $\Lambda$ CDM cosmology, with  $\Omega_{\text{m}} = 0.27$ ,  $\Omega_{\text{b}} = 0.0469$ ,  $h = 0.70$ ,  $n_{\text{s}} = 0.95$ , and  $\sigma_8 = 0.82$ . The simulation has  $2048^3$  particles in a box of  $1h^{-1}\text{Gpc}$  on one side, with particle mass  $8.721 \times 10^9 h^{-1} \text{M}_{\odot}$ . Dark matter haloes are identified with the Rockstar algorithm (Behroozi et al. 2013), which finds haloes through adaptive hierarchical refinement of friends-of-friends groups using the six-dimensional phase-space coordinates and the temporal information.

While the MDR1 simulation is adopted for presenting most of the results, we also make use of the Bolshoi simulation for some investigations that need high completeness in certain regions of the parameter space. The Bolshoi simulation (Klypin et al. 2011)<sup>2</sup> with a  $250h^{-1}\text{Mpc}$  box adopts the same cosmology as MDR1, but with 64 times higher mass resolution and 7 times higher force resolution.

We use the  $z = 0$  Rockstar halo catalogue. In addition to halo mass  $M_{\text{h}}$ ,

for which we adopt  $M_{200\text{b}}$  (i.e. the mean density of a halo being 200 times the background density of the universe), we consider four other halo properties:  $V_{\text{peak}}$ , peak maximum circular velocity of the halo over its accretion history;  $\lambda$ , halo spin parameter that characterises its angular momentum;  $a_{\text{M}/2}$ , cosmic scale factor when the halo obtains half of its current ( $z = 0$ ) total mass, which characterises halo formation time;  $c$ , halo concentration parameter, which is the ratio of the halo virial radius  $R_{\text{vir}}$  to the scale radius  $r_{\text{s}}$ . All the four quantities are related to the halo assembly history and therefore are dubbed as halo assembly variables.

We measure halo bias for haloes above  $\sim 4 \times 10^{11} h^{-1} \text{M}_{\odot}$  (about 50 particles). The large simulation box also serves well our purpose of studying the joint dependence of halo bias on multiple halo properties, as it enables halo bias in fine bins of halo properties to be measured. To further reduce the uncertainty in the halo bias measurements, we derive halo bias from the two-point halo-mass cross-correlation function  $\xi_{\text{hm}}$  and the two-point mass auto-correlation function  $\xi_{\text{mm}}$  (e.g. Jing 1999; Jing et al. 2007), i.e.

$$b(r) = \frac{\xi_{\text{hm}}(r)}{\xi_{\text{mm}}(r)}. \quad (1)$$

In practice, for a given sample of haloes and a pair separation bin  $r \pm dr/2$ , we count the number of halo-mass particle pairs,  $N_{\text{hm}}(r \pm dr/2)$ , and that of mass particle-particle pairs,  $N_{\text{mm}}(r \pm dr/2)$ . With the periodic boundary condition, the corresponding pair counts from randomly distributed haloes and mass particles can be simply calculated as  $N_{\text{hm,ran}}(r \pm dr/2) = n_{\text{h}} n_{\text{m}} V d^3 r$  and  $N_{\text{mm,ran}}(r \pm dr/2) =$

<sup>1</sup> <https://www.cosmosim.org/cms/simulations/mdr1/>

<sup>2</sup> <https://www.cosmosim.org/cms/simulations/bolshoi/>

$n_m^2 V d^3 r/2$ , where  $n_h$  and  $n_m$  are the halo and mass particle number densities in the simulation box of volume  $V$ . The two-point correlation functions are then computed as

$$\xi_{hm}(r) = \frac{N_{hm}(r \pm dr/2)}{N_{hm,ran}(r \pm dr/2)} - 1 \quad (2)$$

and

$$\xi_{mm}(r) = \frac{N_{mm}(r \pm dr/2)}{N_{mm,ran}(r \pm dr/2)} - 1. \quad (3)$$

### 3 JOINT DEPENDENCE OF HALO BIAS ON MASS AND ASSEMBLY VARIABLES

In this section, we first present the results of the joint dependence of halo bias on both mass and one of the assembly variables. Then we investigate whether an effective halo mass can be constructed to absorb the assembly effect in halo clustering. We also discuss how the halo assembly affects the scale dependence of halo bias. Finally, we present the dependence of halo bias on two halo assembly variables at fixed halo mass.

#### 3.1 Dependence of halo bias on mass and one assembly variable

To separate the effects of mass dependence and assembly dependence, we first choose the halo mass bin to have a narrow width,  $\Delta \log M_h = 0.2$ . For each halo mass bin, we further divide haloes into bins of each assembly variable, and typically there are about 20 assembly variable bins. We measure halo bias for haloes in each bin of mass and assembly variable.

We take the average above  $10h^{-1}\text{Mpc}$  as the large-scale halo bias factor, where the ratio between  $\xi_{hm}$  and  $\xi_{mm}$  has become flat.

To maintain reasonable signal-to-noise ratios, we only consider bins with more than 100 haloes.

The joint dependences of halo bias on mass and each assembly variable are shown in Fig. 1.<sup>3</sup> The black curves in each panel delineate the central 50 and 80 per cent of the distribution of the corresponding assembly variable as a function of halo mass.

The lowest mass bin in the investigation is  $\sim 4 \times 10^{11} h^{-1} \text{M}_\odot$ , corresponding to about 50 particles. Paranjape & Padmanabhan (2017) show that for haloes with less than 400 particles, the distribution of halo concentration is not converged (also see Trenti et al. 2010).

3

While the plot does not show the level of uncertainties in the contours, it is clear that the main trend is not affected by noise. The contribution of noise distorts the otherwise smooth contours, showing up as jags in the contour curves or alterations of contour levels (such as the small fluctuation seen in the lower part of the bottom-right panel of Fig. 1). Rather than providing a corresponding plot of the noise levels, we suggest to use the fluctuations in the map as an estimate of the magnitude of noise. This rule of thumb also applies to curve plots, and in general the deviation from a smooth curve gives us the level of noise. However, we do add error bars for a few curves in the curve plots of this paper, and in most cases the noise level is low and the trend is not affected by the noise.

The spin distribution is also affected for haloes with low number of particles (e.g. Trenti et al. 2010; Benson 2017). To see how the resolution effect changes the results, we perform a test (see Appendix A) of replacing haloes of  $\log[M_h/(h^{-1} \text{M}_\odot)] < 12.8$  with those in the Bolshoi simulation, which ensures that each of the lowest mass haloes in our analysis contains more than 3000 particles. We find that the overall trend shown in Fig. 1 still holds. Given the higher signal-to-noise ratio and larger range in assembly variables with the MDR1 simulation, we present the halo bias results using the MDR1 simulation except for the analysis in Section 3.2, where extending to much lower halo mass is needed. For halo pairwise velocity statistics, a caveat is made in Section 4.

The top-left panel shows the joint dependence of halo bias on halo mass  $M_h$  and peak maximum circular velocity  $V_{\text{peak}}$ . At low halo masses halo bias increases as  $V_{\text{peak}}$  increases, while at high halo masses the trend is reversed. The transition mass is around  $\log[M_h/(h^{-1} \text{M}_\odot)] = 13.0$ , which is about three times the nonlinear mass for collapse ( $\log[M_{\text{nl}}/(h^{-1} \text{M}_\odot)] = 12.5$  for the adopted cosmology). Haloes with low mass and high  $V_{\text{peak}}$  have a bias factor comparable to that of high mass haloes, indicating that they could originate from highly stripped high mass haloes (e.g. Wang et al. 2011).

In the top-right panel, it can be seen that at fixed mass haloes formed earlier (i.e. with lower  $a_{M/2}$ ) are more strongly clustered. The trend becomes weak for haloes above  $\sim 10^{14} h^{-1} \text{M}_\odot$ , manifested by the almost vertical contours. Extremely old haloes (the bottom boundary in the panel) at all masses are all as strongly clustered as massive haloes.

At fixed mass, old haloes tend to be more concentrated, i.e. with higher concentration parameters  $c$ . The dependence of halo bias on concentration (bottom-left panel) follows a similar trend as with formation time (see § 3.4 for the condition for this to be valid). The dependence becomes weak around  $3M_{\text{nl}}$ , which is consistent with previous work

of direct measurements by binning halo concentration (e.g. Wechsler et al. 2006; Jing et al. 2007) and high precision inference with a lognormal model and Separate Universe technique (Paranjape & Padmanabhan 2017). We note that the latter shows concentration-dependent assembly bias as a function of the actual value of concentration, instead of percentiles of concentration.

However, at higher halo masses, halo bias decreases with increasing halo concentration, clearly different from that in the  $a_{M/2}$  case. This difference implies that halo concentration  $c$  can depend on quantities other than formation time ( $a_{M/2}$ ), like the mass accretion rate (e.g. Wechsler et al. 2002).

In the bottom-right panel, the joint dependence of halo bias on halo mass and spin is shown. The distribution of halo spin (indicated by the black curves) is only weakly dependent on halo mass. Overall the contours show an ordered pattern (except for the extremely low spin tail of low mass haloes), with haloes of higher spin more strongly clustered. Unlike the cases in the other three panels, the trend persists over all halo masses, which is consistent with the result using percentiles of spin distribution (Gao & White 2007).

Compared to studies of halo bias for haloes selected from percentiles of assembly variables, our results show clearly the joint dependence of halo bias as a function of halo

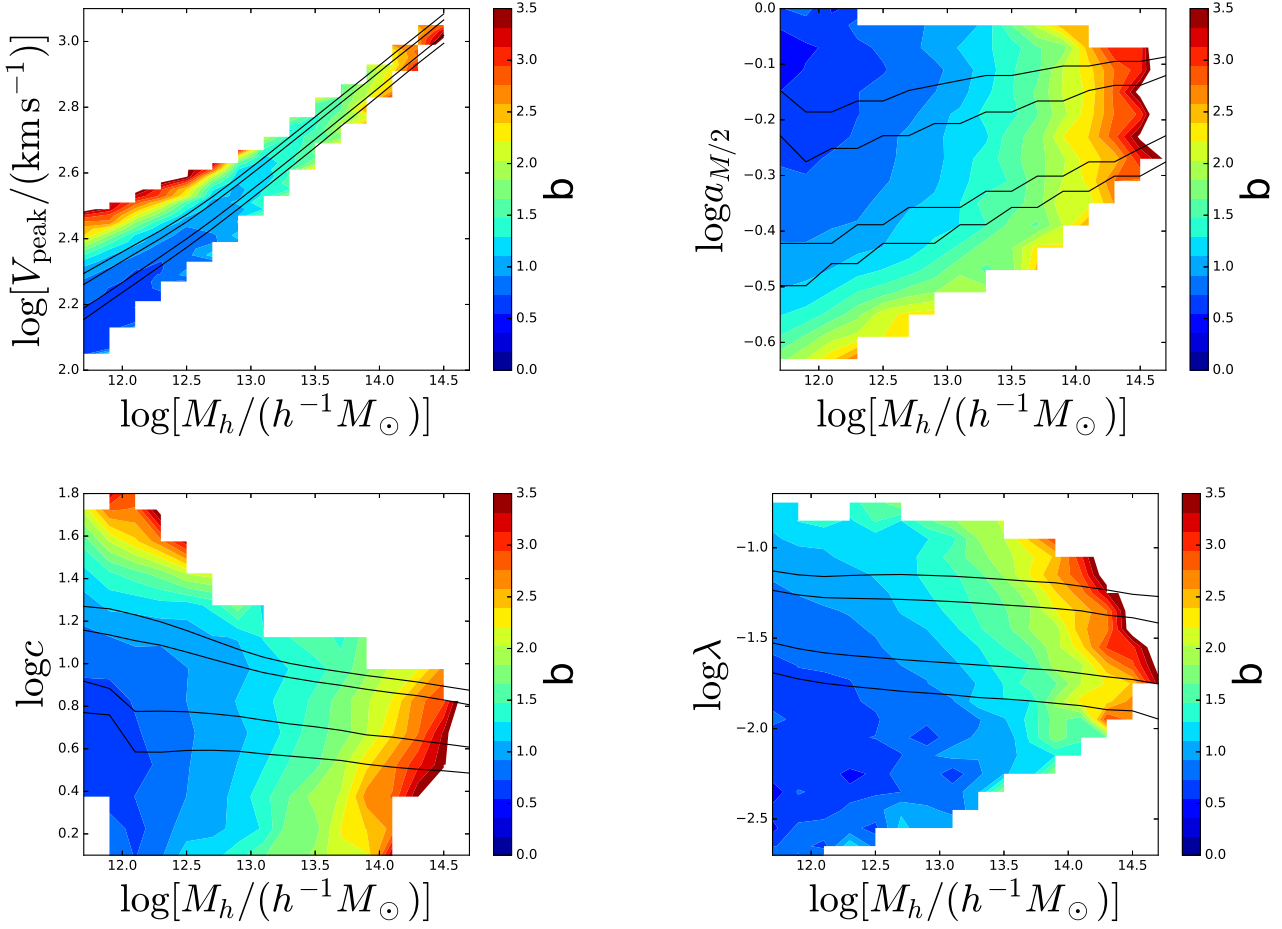


**Figure 1.** Joint dependence of halo bias on halo mass and each assembly variable. The assembly variables in the four panels are peak maximum circular velocity  $V_{\text{peak}}$ , halo formation scale factor  $a_{M/2}$ , halo concentration  $c$ , and halo spin  $\lambda$ , respectively. The four black curves in each panel mark the central 50 and 80 per cent of the distribution of the corresponding assembly variable as a function of halo mass.

mass and the value of each assembly variable. In the  $M_h$ – $A$  ( $A$  being one of the assembly variable) plane, the common description of our results can be that halo bias increases outward from a point of global minimum. Such a description is not obvious if the investigation is limited to the main distribution range of the assembly variable. The previous results can all be understood by considering slices in the  $M_h$ – $A$  plane and by noticing the shape and orientation of the contours.

With the above description motivated by our calculation, it would be interesting to ask whether we can define a new halo variable to account for both the halo mass and assembly history dependences of halo bias. We do such an exercise below.

### 3.2 Effective mass to absorb the assembly bias effect?

To see whether we can construct a halo variable from combinations of halo mass and assembly variables to minimise the assembly history effect on halo bias, we investigate an example with halo mass  $M_h$  and spin  $\lambda$ . As shown in Fig. 1, the distribution of halo spin is almost independent of halo

mass and the joint dependence of halo bias on  $M_h$  and  $\lambda$  has a pattern easy to describe.

Within the most part of the parameter space extended by  $\log M_h$  and  $\log \lambda$ , a given value of halo bias factor approximately corresponds to a straight line (see the dashed lines in Fig. 2 as examples). We find that the set of straight lines can be well described as converged to a single point ( $\log M_{h,0}$ ,  $\log \lambda_0$ ), located towards the bottom-right corner of the left panel of Fig. 2. The slope  $(\log M_h - \log M_{h,0})/(\log \lambda - \log \lambda_0)$  of each line can be defined as a new halo variable, which is a combination of halo mass  $M_h$  and spin  $\lambda$ . Halo bias is monotonically dependent on this variable. Equivalently, for each line, we can evaluate the halo mass at a fixed spin value and use this halo mass as the new variable. We choose the fixed spin value to be  $\log \lambda_{\text{eff}} = -1.4$ , roughly the value averaged over all haloes, and define the corresponding halo mass as the effective halo mass  $M_{\text{eff}}$  through

$$\log M_{\text{eff}} = \log M_{h,0} + \frac{\log \lambda_{\text{eff}} - \log \lambda_0}{\log \lambda - \log \lambda_0} (\log M_h - \log M_{h,0}). \quad (4)$$

To cover a large range in effective halo mass, we perform the analysis using a combination of haloes in both the MDR1 and Bolshoi simulations. As seen from Fig. 2, for

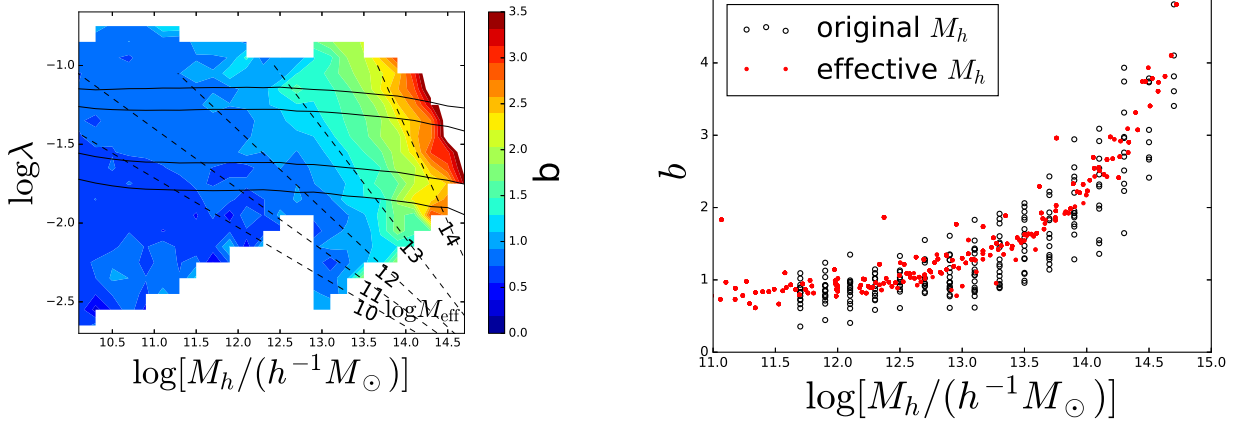


**Figure 2.** Effective halo mass to absorb assembly bias effect with halo spin. The left panel is the same as the bottom-right panel of Fig. 1, and dashed lines are added to illustrate how the effective mass is defined (see text). In the right panel, the black points show the halo bias as a function of halo mass, with the scatter at fixed halo mass coming from haloes with different spin parameters (assembly bias effect with spin). The red points show the dependence of halo bias on effective halo mass, and the scatter caused by the assembly effect with spin is substantially reduced.

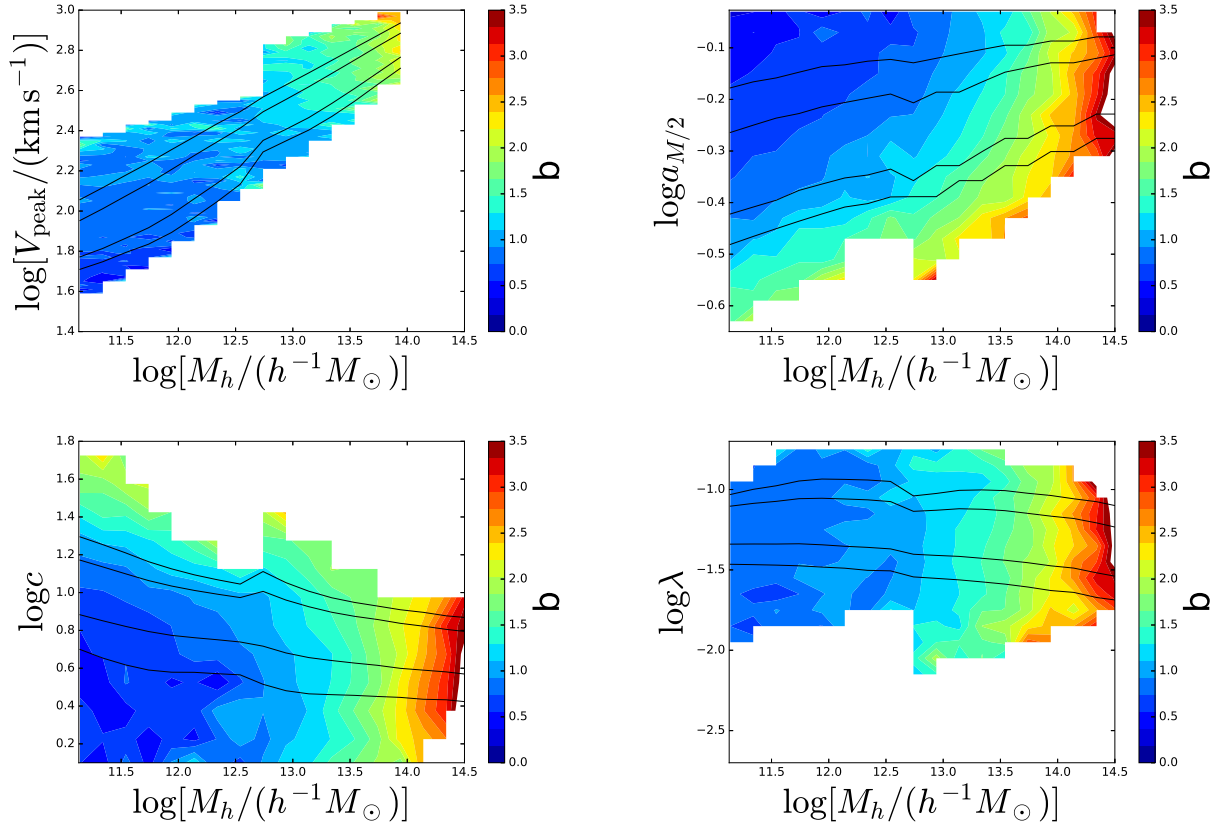


**Figure 3.** Same as Fig. 1, but with original halo mass replaced by effective halo mass. The effective halo mass absorbs the halo assembly bias with halo spin, manifested by the vertical contours in the bottom-right panel. However, assembly bias effect still exists with other assembly variables, as seen in the other three panels.



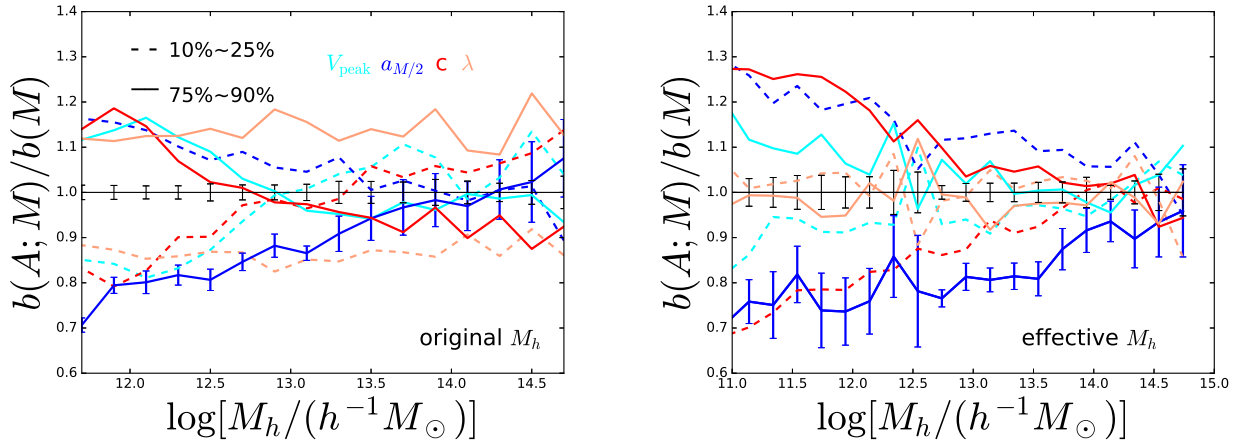


**Figure 4.** Comparison between assembly bias effects under original halo mass (left) and effective halo mass (right). At fixed original or effective halo mass, haloes are grouped according to the percentiles of each assembly variable, and their bias values normalised by the mass-only dependent bias are shown as curves in each panel (dashed for the 10–25 per cent percentile and solid for the 75–90 per cent percentile).

an effective mass of  $\log[M_{\text{eff}}/(h^{-1}M_{\odot})] \sim 11\text{--}12.5$ , we have contributions from haloes of mass below  $\log[M_h/(h^{-1}M_{\odot})] \sim 11.6$  with high spin. Furthermore, there is numerical effect for haloes with less than a few hundred particles (e.g. Paranjape & Padmanabhan 2017; Trenti et al. 2010; Benson 2017) in the MDR1 simulation. To include low mass haloes and minimise the potential numerical effect, we calculate effective halo masses for both MDR1 and Bolshoi haloes, then present the results using MDR1 haloes for  $\log[M_{\text{eff}}/(h^{-1}M_{\odot})] \geq 12.7$  and Bolshoi haloes for  $\log[M_{\text{eff}}/(h^{-1}M_{\odot})] < 12.7$ .

To verify that the effect of assembly bias in spin is absorbed into the effective halo mass, we measure halo bias in fine bins of  $\log M_{\text{eff}}$  and  $\log \lambda$ . In the right panel of Fig. 2, the black circles show the dependence of halo bias on the original halo mass  $M_h$ , and the spread at fixed mass reflects the assembly bias effect in halo spin. The red dots represent the dependence of halo bias on the effective halo mass  $M_{\text{eff}}$ . At fixed  $M_{\text{eff}}$  the scatter is much smaller than that seen in the  $b\text{--}M_h$  dependence, demonstrating that the assembly bias effect in spin has been well absorbed into the effective mass.

Fig. 3 is similar to Fig. 1, but for the joint dependence of halo bias as a function of effective mass  $M_{\text{eff}}$  and each of the assembly variable. The fact that the assembly bias effect in spin has been absorbed into  $M_{\text{eff}}$  shows up as largely vertical contours in the  $\log M_{\text{eff}}\text{--}\log \lambda$  plane (bottom-right panel).

However, in the other three panels of Fig. 3, where the joint dependence of halo bias on  $M_{\text{eff}}$  and the other assembly variables are shown, assembly bias still exists at fixed  $M_{\text{eff}}$ . The assembly bias effect becomes weaker at the high  $M_{\text{eff}}$  end. This is not surprising, given that the effect is weak at high  $M_h$  in Fig. 1 and the  $\lambda$  dependence appears to be the strongest one.

In Fig. 4, we show the assembly bias effect as a function of the original halo mass (left panel) and the effective halo mass (right panel), by grouping haloes into 10–25 per cent and 75–90 per cent percentiles of different assembly variables. Error bars are calculated with the jackknife method. For clarity, we only plot error bars for  $b(M)$  (black solid)

and  $a_{M/2}$  (dark blue). Under the effective halo mass, the assembly bias in halo spin almost disappears, and the curves of bias from the two percentile subsamples fall on top of each other (on the line of unity, corresponding to the average bias as a function of effective mass), while under the original halo mass the assembly effect in halo spin is at the level of  $\sim 15$  per cent. Above  $\log[M_{\text{eff}}/(h^{-1}M_{\odot})] \sim 13.5$ , the assembly effects in  $V_{\text{peak}}$  and  $c$  are also reduced, but not in  $a_{M/2}$ . However, towards lower  $M_{\text{eff}}$ , the assembly bias effect in other assembly variables becomes enhanced, compared to the case with the original halo mass. Therefore, the effective mass does not work all the way to reduce assembly bias effect in other variables and over the full mass range.

With the joint dependence of halo bias on  $M_{\text{eff}}$  and assembly variables, in principle we can perform a similar variable transformation to largely reduce the assembly effect in another chosen variable, and the analysis can be repeated until the assembly effect in all the assembly variables of interest is recursively absorbed. It may be possible to find a principal direction or locus in the multidimensional space spanned by halo mass and assembly variables such that halo bias has the strongest dependence on the corresponding variable combination. However, there is a limit on how far we would like to go following such a path. If the ultimate goal is to replace halo mass with the putative variable combination in halo modelling of galaxy clustering, it is desirable that the variable combination has a tight correlation with galaxies properties. It has been established that halo mass plays the dominant role in shaping galaxy formation and evolution and in determining the main properties of galaxies (e.g. White & Rees 1978; Birnboim & Dekel 2003; Kereš et al. 2005). Although the combination variable  $M_{\text{eff}}$  absorbs the assembly bias effect in halo spin, a fixed  $M_{\text{eff}}$  spans a large range in halo mass. For example, haloes of effective mass  $M_{\text{eff}} = 10^{12} h^{-1} M_{\odot}$ , which corresponds to the middle dashed line in the left panel of Fig. 2, can come from haloes of original mass  $M_h \sim 10^{11} h^{-1} M_{\odot}$  with high spin or those of  $M_h \sim 10^{13} h^{-1} M_{\odot}$  with low spin. The large range in original halo mass suggests that  $M_{\text{eff}}$  would not be a good

variable to choose for a tight correlation with galaxy properties. Together with the results in Fig. 3 and Fig. 4, it implies that it is unlikely to find the right combination of halo variables to completely absorb the assembly bias effect in every assembly variable and at the same time to keep a close connection to galaxy properties.

### 3.3 Scale dependence of halo bias with assembly variable

While the assembly history of haloes affects large-scale clustering, it can also have an effect on small-scale clustering. In Fig. 5, the scale dependences of halo bias on assembly variables are shown at two halo masses,  $\log[M_h/(h^{-1}M_\odot)] = 12$  and 14, respectively. The top eight panels show the original bias factors  $b(A; r)$  as a function of  $r$ , calculated by grouping haloes into various percentiles of each assembly variable  $A$ . To emphasise the shape difference on small scales, in the bottom eight panels we also show halo bias factors normalised by the corresponding large-scale value (average values above  $10h^{-1}\text{Mpc}$ ), i.e.  $b(A; r)/\langle b(A; r > 10h^{-1}\text{Mpc}) \rangle$ . For clarity, in each panel, error bars are only plotted for the curve corresponding to all haloes to indicate the uncertainties.

In the non-normalised case, for  $M_h = 10^{12}h^{-1}M_\odot$  haloes, all halo bias factors (solid curves in the top panels) start to drop at  $\sim 3h^{-1}\text{Mpc}$  towards small scales, which means that the two-point halo-mass cross-correlation function is shallower than the mass auto-correlation function on such scales. Note that the drop occurs on scales larger than the halo virial radius ( $R_{\text{vir}} \sim 0.21h^{-1}\text{Mpc}$ ). The panels show that halo assembly history influences how steep the bias factor drops towards small scale. Except for the halo spin case, all other cases have a similar trend that can be related through the correlation between halo assembly variables. Haloes that form earlier (smaller  $a_{M/2}$ ), thus on average with higher halo concentration  $c$  and higher  $V_{\text{peak}}$ , have a steeper drop in halo bias towards smaller scales. The dotted curves in each panel are the measurements of halo bias using halo-halo auto-correlation functions, and the trend is similar to that derived from halo-mass cross-correlation functions.

For the case with halo spin, the overall shape difference is smaller than seen in other three cases. As halo spin shows an anti-correlation with halo concentration (e.g. Macciò et al. 2007; also Fig. 6 and Fig. 7), one would expect the trend to be that the scale-dependent bias for haloes with lower spin drops more steeply towards smaller scales. However, the result is opposite (see § 3.4 for an interpretation).

The bottom panels of the non-normalised case in Fig. 5 show the results with  $M_h = 10^{14}h^{-1}M_\odot$  haloes. As the virial radius  $R_{\text{vir}}$  is  $\sim 0.98h^{-1}\text{Mpc}$ , the rise on small scales reflects the mass distribution inside haloes. For all cases, the dotted curves for halo biases from halo-halo auto-correlation functions have a cutoff around  $r \sim 2R_{\text{vir}}$ , a manifestation of the halo exclusion effect. Above  $\sim 2R_{\text{vir}}$ , the shape of scale-dependent halo bias factors do not show a strong dependence on assembly variables (shown more clearly in the corresponding panels for the normalised case).

Overall the shape of the scale dependence of halo bias at small scales depend on the value of the assembly variable in consideration, as shown in the normalised case. The dependence is not strong, but it is discernible for low mass haloes. For high mass haloes, the dependence becomes weak (except

for the spin case). In such a situation, the scale-dependent assembly bias at a given halo mass  $M_h$  can be well approximated as  $b(M_h, A; r) = \langle b(M_h, A) \rangle f(M_h; r)$ , where  $\langle b(M_h, A) \rangle$  is the large-scale bias with the value of assembly variable being  $A$  and  $f(M_h; r)$  characterise the shape (being unity on large scales by construction).

Sunayama et al. (2016) study the scale dependence of halo assembly bias for the case of  $V_{\text{max}}$ , the maximum circular velocity at  $z = 0$ . They find that for low-mass haloes ( $M_h \lesssim M_{\text{nl}}$ ) the ratio of biases between high  $V_{\text{max}}$  and low  $V_{\text{max}}$  haloes exhibits a pronounced scale dependence at  $0.5\text{--}5h^{-1}\text{Mpc}$ , and the scale dependence becomes weak towards higher halo mass. Our results, if put in a similar format, are in broad agreements with their findings. They also show that the scale dependence can be partially attributed to haloes previously residing in higher mass haloes but ejected to become host haloes at the epoch of interest, which is consistent with the proposed origin of assembly bias for low mass haloes (e.g. Wang et al. 2009; Wetzel et al. 2014).

If galaxy properties track the halo assembly history, the scale-dependent bias from the halo assembly effect could be a way to reveal the assembly bias in galaxy clustering. However, the results in Fig. 5 show that the scale dependence from assembly effect is not strong, and the overall shape does not vary significantly with the magnitude of any assembly variables, at a level of  $\sim 10$  per cent on scales around  $3h^{-1}\text{Mpc}$  for low mass haloes (see the normalised curves in Fig. 5). Also on scales where the scale dependence has a relatively large amplitude, the one-halo contribution to the galaxy correlation function would tend to mask it. Therefore, in practice, it is probably difficult to discern the assembly effect from the scale dependence in galaxy clustering.

### 3.4 Dependence of halo bias on two assembly variables

At fixed halo mass, Fig. 1 shows the dependence of halo bias on each assembly variable. While in general assembly variables are correlated with each other, there are differences in the assembly bias trends with different assembly variables. To better understand the trends, we present the correlation between any two assembly variables and how halo bias depends on them at fixed halo mass.

Each panel of Fig. 6 shows halo bias as a function of two assembly variables, measured with haloes of mass in the range  $\log[M_h/(h^{-1}M_\odot)] = 12.5 \pm 0.5$  (i.e. about  $M_{\text{nl}}$ ). The contours enclose the 68 and 95 per cent distribution of the two assembly variables, respectively, which also reveal the correlation between them. As can be seen in the top-left panel, halo concentration  $c$  and formation scale factor  $a_{M/2}$  are anti-correlated, i.e. older haloes are more concentrated. The gradient of the halo bias follows the correlation direction. In such a case, the trend of dependence of halo bias on one variable can be used to predict that on the other variable. For example, at the above mass, given that more concentrated haloes are more strongly clustered and generally older, we can infer that older haloes are more strongly clustered than younger haloes. This is indeed what is seen in Fig. 1. Besides  $c\text{--}a_{M/2}$ , the bias dependences on  $c\text{--}V_{\text{peak}}$  (top-middle panel) and  $V_{\text{peak}}\text{--}a_{M/2}$  (top-right panel) also follow a similar behaviour.

However, as halo spin  $\lambda$  becomes involved, the above

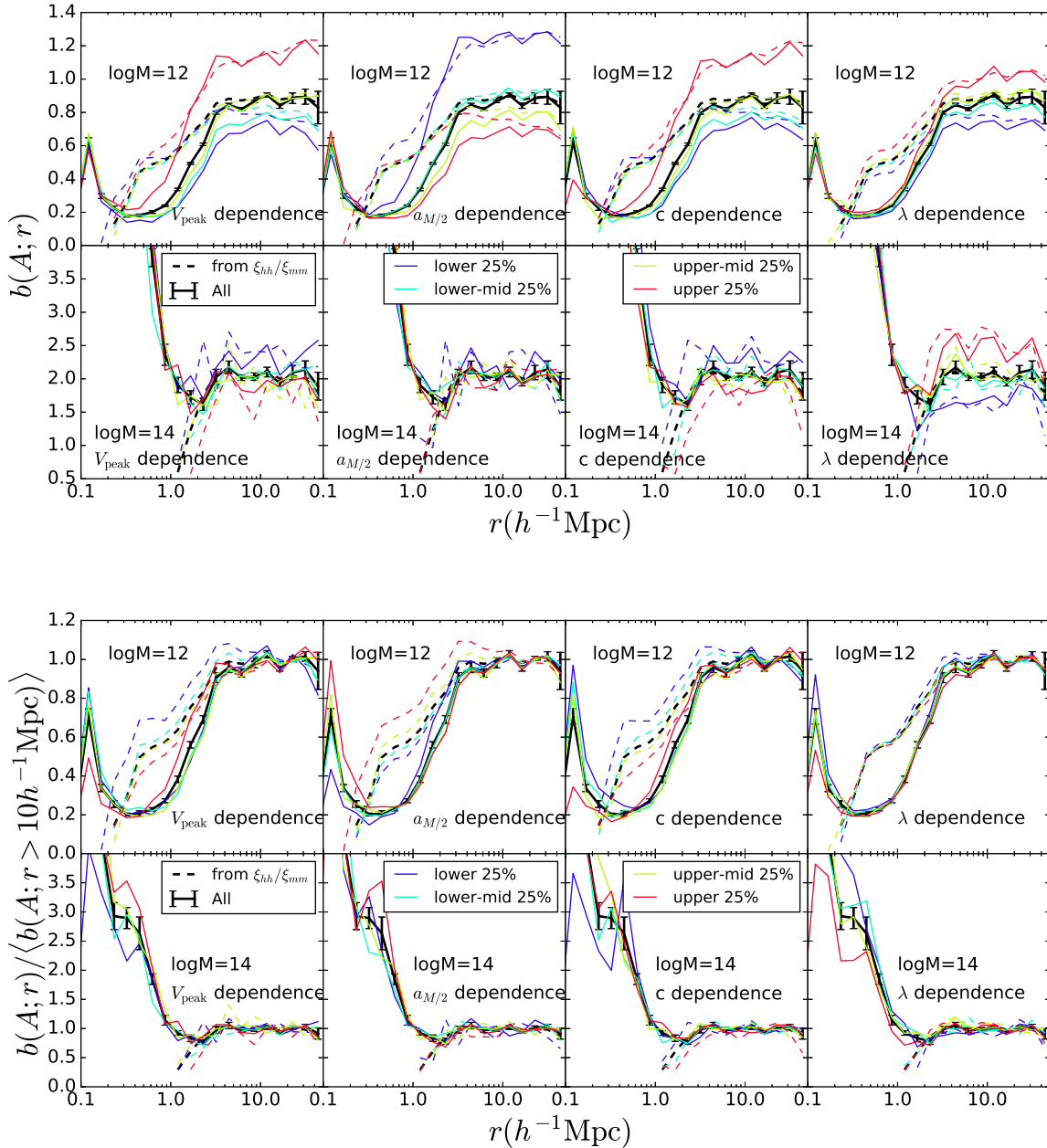


**Figure 5.** Scale dependence of assembly bias. The upper subplot shows the scale-dependent halo bias factor for different assembly variables. In each panel, solid curves are calculated through halo-mass cross-correlation functions and dotted curves through halo-halo auto-correlation functions. Each set of five curves are for haloes in different percentiles of each assembly variable: lower 25 per cent (blue), lower-middle 25 per cent (cyan), upper-middle 25 per cent (green), upper 25 per cent (red), and all haloes in the mass bin (black). Top and bottom panels are for haloes of  $\log[M_h/(h^{-1}M_\odot)]=12$  and 14, respectively. Bottom subplot is similar, but each halo bias curve is normalised by the corresponding large-scale value (average on scales larger than  $10h^{-1}\text{Mpc}$ ).

picture changes. For example, in the bottom-right panel, halo spin  $\lambda$  is positively correlated with  $a_{M/2}$ , meaning that haloes of lower spin are generally older. Unlike the previous cases, now the gradient of the halo bias is not along the correlation direction but about perpendicular to it, and the correlation can no longer be used to predict the bias dependence trend. That is, the fact that older haloes are more strongly clustered and have a lower spin does not im-

ply that haloes of lower spin are more strongly clustered. In this example, the contrary is true (haloes of lower spin are less clustered as seen in the panel and in Fig.1).

The difference between the halo bias gradient and the correlation direction with two assembly variables can help resolve apparent puzzles in assembly bias trend with other variables, e.g. the dependence on halo age and the number of subhaloes (above some mass threshold). The occupa-



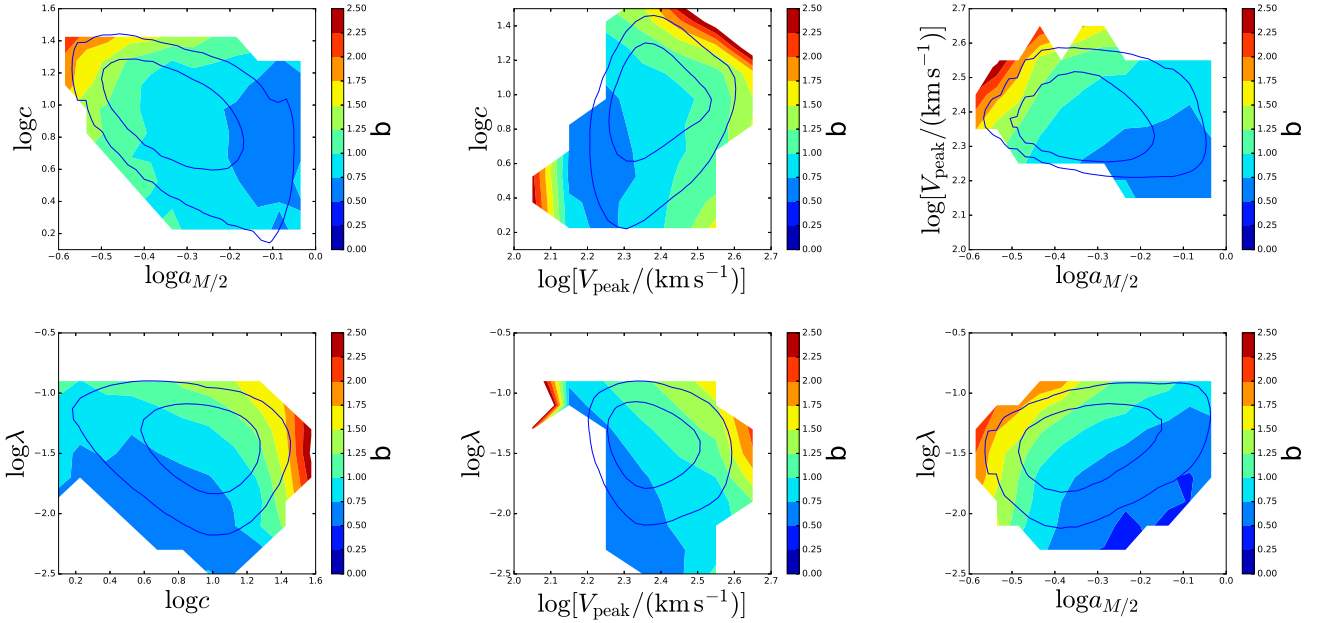


**Figure 6.** Halo bias as a function of two assembly variables for haloes in the mass range of  $\log[M_h/(h^{-1}M_\odot)] = 12.5 \pm 0.5$ . In each panel, the contours mark the 68 per cent and 95 per cent distribution of the two assembly variables and the colour scale shows the value of halo bias.

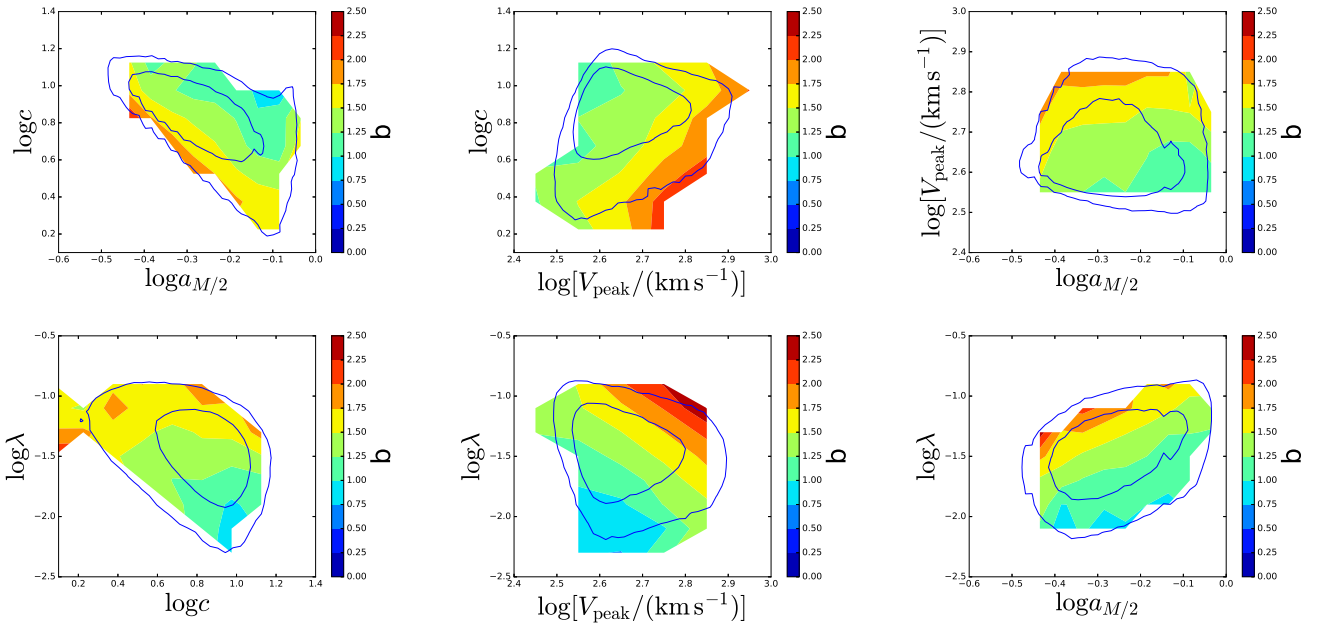


**Figure 7.** Same as Fig. 6, but for haloes in the mass range of  $\log[M_h/(h^{-1}M_\odot)] = 13.5 \pm 0.5$ .

tion number of subhaloes is found to correlate with halo age in the sense that older haloes have fewer subhaloes (e.g. Gao et al. 2004), resulting from dynamical evolution and destruction of subhaloes. As in the mass range considered here older haloes are more strongly clustered, the correlation would imply haloes of fewer subhaloes are more strongly clustered. However, the dependence on subhalo occupation number is found to be opposite to such a naive expectation (e.g. Croft et al. 2012).

Fig. 7 shows halo bias as a function of two assembly variables for massive haloes ( $\log[M_h/(h^{-1}M_\odot)] = 13.5 \pm 0.5$ , above  $M_{\text{nl}}$ ). Compared to the case with low mass haloes (Fig. 6), while the correlation between each two assembly variables does not change much, the direction of the gradient of halo bias can be substantially different. For example, the gradient direction in the  $c$ - $a_{M/2}$  panel now becomes perpendicular to the correlation direction. As a consequence, the trend in assembly bias effect and its relation to the correlation also

changes. For cases involving halo spin, the gradient direction has only a mild change, indicating that the origin of spin bias is different from others (e.g. Salcedo et al. 2018).

With the Separate Universe technique, Lazeyras et al. (2017) present the dependence of halo bias on two assembly variables in two halo mass bins, although the dependence is not compared with the correlation of each two variables. They show that the dependence changes with halo mass and the trend is weak if halo shape is used as one variable. Han et al. (2018) present analysis of the multidimensional dependence of bias on halo properties. Their results, if projected onto the space of two assembly variables at fixed halo mass, can be compared to ours.

Overall we see that the joint dependence of halo bias on two assembly variables does not necessarily follow the correlation between the variables. One should be cautious in inferring assembly bias trend in one variable based on its correlation to the other variable. A similar conclusion is reached by Mao et al. (2018) for the so-called “secondary bias” with cluster-size haloes. The pattern of the joint dependence varies with halo mass, which can be characterised by a rotation (e.g. in terms of the halo bias gradient) as halo mass increases.

#### 4 DEPENDENCE OF PAIRWISE VELOCITY AND VELOCITY DISPERSIONS ON HALO ASSEMBLY

The assembly bias from the spatial distribution or clustering of haloes is related to halo environment, which should also affect the velocity distribution of haloes. The velocity distribution of haloes is a major ingredient in modelling redshift-space clustering of galaxies. To yield insights on how halo assembly may affect redshift-space clustering, we investigate the halo assembly effect on halo velocity distribution.

We present the results in terms of halo pairwise velocity,  $\mathbf{v}_{12} = \mathbf{v}_2 - \mathbf{v}_1$ , as a function of halo pair separation,  $r = |\mathbf{r}_{12}| = |\mathbf{r}_2 - \mathbf{r}_1|$ , where  $\mathbf{v}_i$  and  $\mathbf{r}_i$  ( $i=1, 2$ ) are the velocities and positions of a pair of haloes. The pairwise radial and transverse velocities are calculated as  $\mathbf{v}_{12,r} = (\mathbf{v}_{12} \cdot \mathbf{n}_{12})\mathbf{n}_{12}$ , and  $\mathbf{v}_{12,t} = \mathbf{v}_{12} - \mathbf{v}_{12,r}$ , where  $\mathbf{n}_{12} = \mathbf{r}_{12}/|\mathbf{r}_{12}|$  is the direction from one halo to the other of the pair. The corresponding velocity dispersions are  $\sigma_{12,r} = \langle v_{12,r}^2 \rangle - \langle v_{12,r} \rangle^2$  and  $\sigma_{12,t} = \langle v_{12,t}^2 \rangle - \langle v_{12,t} \rangle^2$ , with the average over all halo pairs at a given separation  $r$ .

Before moving on to present the results on pairwise velocity statistics, we point out the comparison between those from the Bolshoi and MDR1 simulations (see Appendix A). In general, the MDR1 results in similar dependence patterns of the pairwise velocity statistics on assembly variables, except for halo spin. The weak trend with spin seen in the MDR1 simulation does not show up in the Bolshoi simulation, which may be caused by noise in the Bolshoi simulation or unknown systematic effect in determining halo spin in low-resolution simulations. For consistency, we choose to present the MDR1 results with the above caveat for the spin results (more details in Appendix A).

#### 4.1 Assembly effect on pairwise velocity of haloes

In Fig. 8, we first show the halo mass dependent pairwise velocity and velocity dispersions, as a function of halo pair separation. Consistent with previous study (e.g. Zheng et al. 2002), the pairwise infall velocity  $v_{12,r}$  (left panel) increases as halo mass increases, and the increase is faster at smaller pair separation, reflecting the stronger gravitational influence from higher mass haloes. For high mass haloes (with mass above a few times  $M_{\text{nl}}$ ), the pairwise radial velocity continuously decreases toward large separation. For low mass haloes, a bump in the pairwise radial velocity shows up. The bump is around  $r \sim 5h^{-1}\text{Mpc}$  for haloes of the lowest mass in the study and shifts to larger scales for haloes of higher mass. At large separation, the pairwise infall velocity tends to converge to an amplitude independent of halo mass, which reflects the fact that all haloes feel the same large-scale gravitational potential field sourced by linear fluctuations.

The pairwise radial velocity dispersion  $\sigma_{12,r}$  (middle panel) decreases toward small halo pair separation. The dependence on halo mass is weak – in the range of  $r \sim 1\text{--}5h^{-1}\text{Mpc}$ , lower mass haloes have slightly higher  $\sigma_{12,r}$ . The dispersion  $\sigma_{12,t}$  of the pairwise transverse velocity (right panel) has a similar trend. On large scales, the one-dimensional (1D) pairwise transverse velocity dispersion  $\sigma_{12,t}/\sqrt{2}$  (right panel) is about 10 per cent lower than the radial one (middle panel).

In Fig. 9, the dependence of pairwise radial velocity (top panel) and the radial and transverse velocity dispersions (middle and bottom panels) on assembly variables are shown for haloes of  $\log[M_h/(h^{-1}M_\odot)] = 11.73$ . Below  $\sim 1h^{-1}\text{Mpc}$ , the pairwise radial velocity does not show a strong dependence on any of the assembly variable. Above  $\sim 1h^{-1}\text{Mpc}$ , the assembly effect becomes clear. Both radial and transverse pairwise velocity dispersions show a substantial dependence on assembly variables at all scales. To see the trend more clearly, Fig. 10 shows the dependences by grouping each assembly variable into four percentiles. For the radial pairwise velocity, the bump around  $r \sim 5h^{-1}\text{Mpc}$  seen in Fig. 8 shows up for each group, and the scatter caused by assembly effect also reaches maximum at this scale. The assembly effect in pairwise velocity with halo spin is not as strong as with other assembly variables, opposite to the trend seen in halo bias (e.g. left panel of Fig. 4).

For low-mass haloes presented here, similar to the spatial clustering, the trend of the dependence of pairwise velocity on assembly variables follows the correlations among assembly variables, except for the case with halo spin. At fixed mass, haloes that on average form earlier (with lower  $a_{M/2}$ , higher  $c$ , or higher  $V_{\text{peak}}$ ) have higher pairwise velocity and velocity dispersions. This is in line with the evolution of those low-mass haloes being influenced by the surrounding environment, especially the tidal field (e.g. Hahn et al. 2007, 2009; Wang et al. 2011; Shi et al. 2015) and with some of them being ejected haloes around massive haloes (e.g. Wang et al. 2009; Wetzel et al. 2014). The deviation between the pairwise velocity trend with halo spin and the expectation from correlations with other assembly variables arises from the misalignment of the gradient of pairwise velocity and the direction of the correlation in the plane of spin and one other assembly variable, similar to what we discuss in § 3.4 for halo bias.

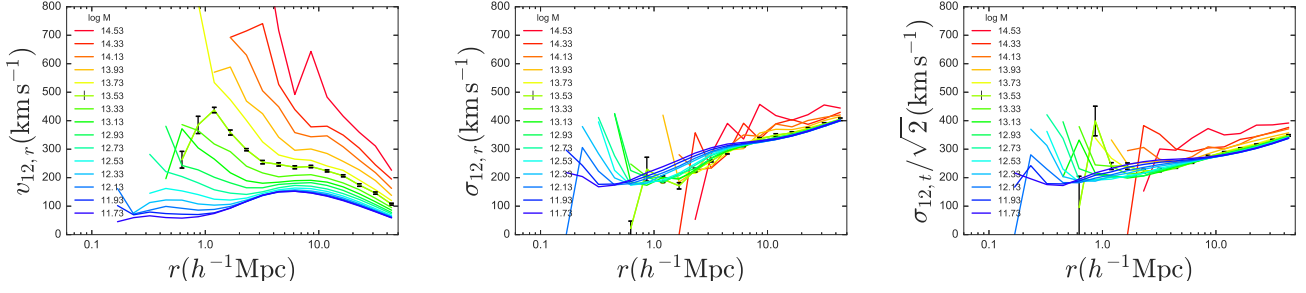


**Figure 8.** Pairwise velocity and velocity dispersions of haloes. The left panel shows the scale-dependent pairwise radial velocity as a function of halo mass. The middle and right panels are similar, but for pairwise radial and transverse velocity dispersions, respectively.

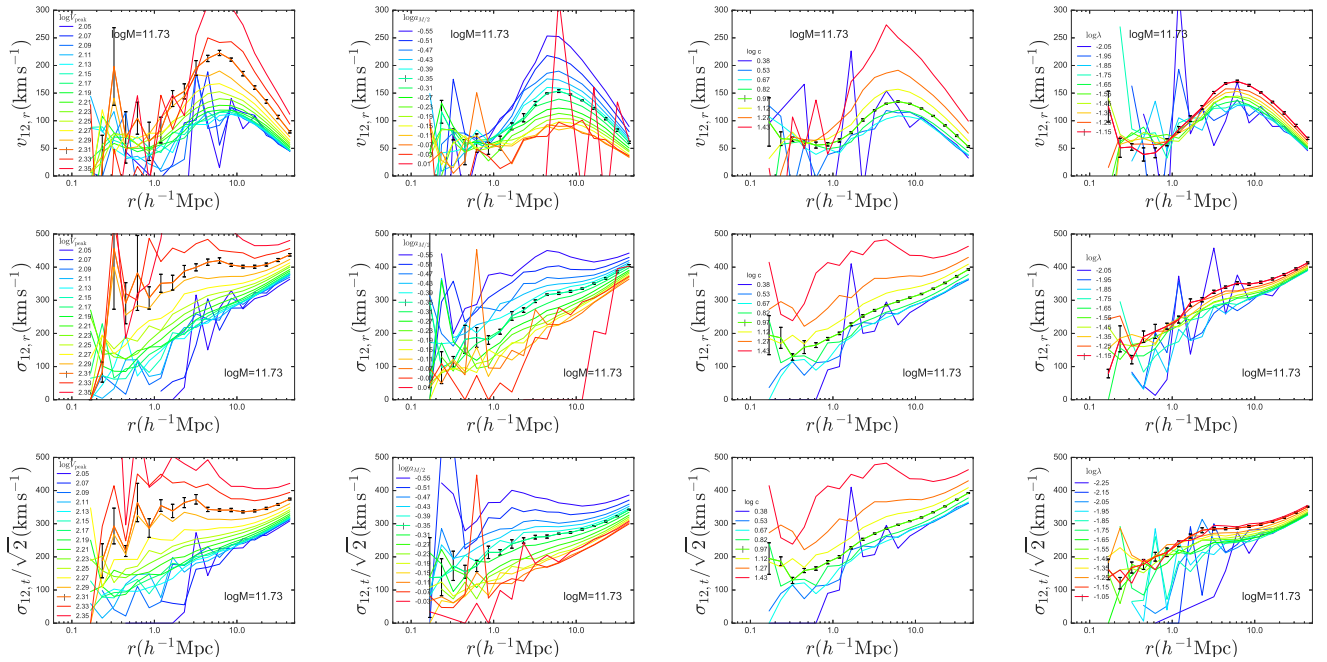


**Figure 9.** Dependence of halo pairwise velocity and velocity dispersions on assembly variables for low-mass haloes ( $\log[M_h/(h^{-1}M_\odot)] = 11.73$ ). Top, middle, and bottom panels show pairwise radial velocity, pairwise radial velocity dispersion, and pairwise transverse velocity dispersion, respectively. In each panel, the curves are colour coded according to the value of the corresponding assembly variable.

For the joint dependence of pairwise velocity and velocity dispersions on halo mass and each assembly variable, we plot  $v_{12,r}$ ,  $\sigma_{12,r}$ , and  $\sigma_{12,t}/\sqrt{2}$  at the scale  $r \sim 5h^{-1}\text{Mpc}$  in Fig. 11. The trend is similar to the joint dependence for halo bias (Fig. 1), and at fixed mass, more strongly clustered haloes display higher pairwise velocity and velocity dispersions.

#### 4.2 Relation between spatial clustering and pairwise velocity under assembly effect

The overall pattern of pairwise velocity and velocity dispersions in Fig. 11 shows a clear correlation with that of halo bias in Fig. 1. With the joint effect of halo mass and assembly, more strongly clustered haloes tend to move faster with higher velocity dispersions. Such a correlation motivates us to further study the relation between spatial clustering and halo velocity field.

Under the assumption that halo pairs are conserved dur-

ing evolution, a relation can be established between halo pairwise velocity and spatial clustering. On large scales, halo pairwise velocity is found to be proportional to halo bias (e.g. Sheth et al. 2001b; Zhang & Jing 2004),  $v_{12,r} \propto b$ . This would have interesting implications for the assembly effect. For example, in the low halo mass regime, if all older haloes originate from stripped massive haloes so that their stronger clustering is a manifestation of that of more massive haloes, their pairwise velocity should also follow that of the massive haloes. We would expect a tight correlation between  $v_{12,r}$  and  $b$  for all subsets of haloes (divided according to mass and assembly history).

In the top panels of Fig. 12, the values of  $v_{12,r}$  around  $r \sim 10h^{-1}\text{Mpc}$  and halo bias  $b$  are plotted for halo subsamples in bins of halo mass and assembly variables.

In each panel, the colour indicates the halo mass and the size of the points denotes the magnitude of the assembly variable. We note that the magnitude of the assembly bias is not the focus here. At fixed mass it is simply related to

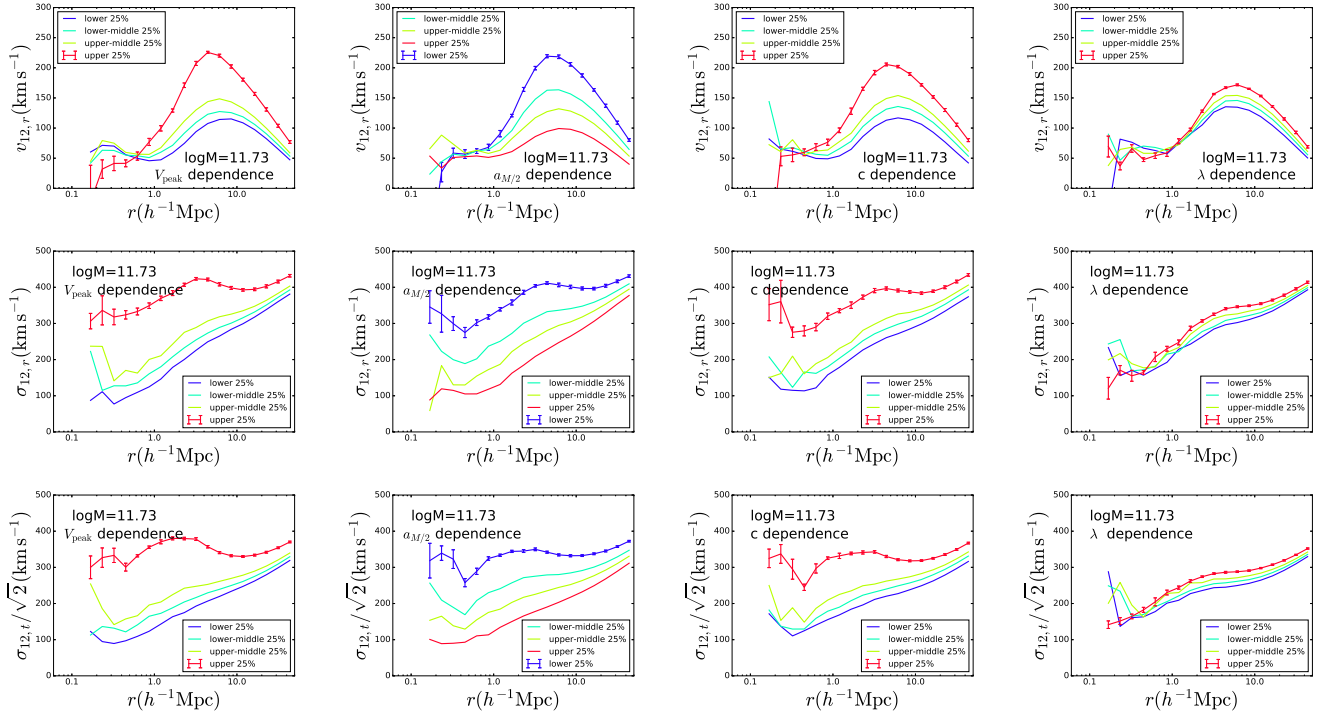


**Figure 10.** Same as Fig. 9, but in each panel the curves are colour coded according to the percentile of the corresponding assembly variable.

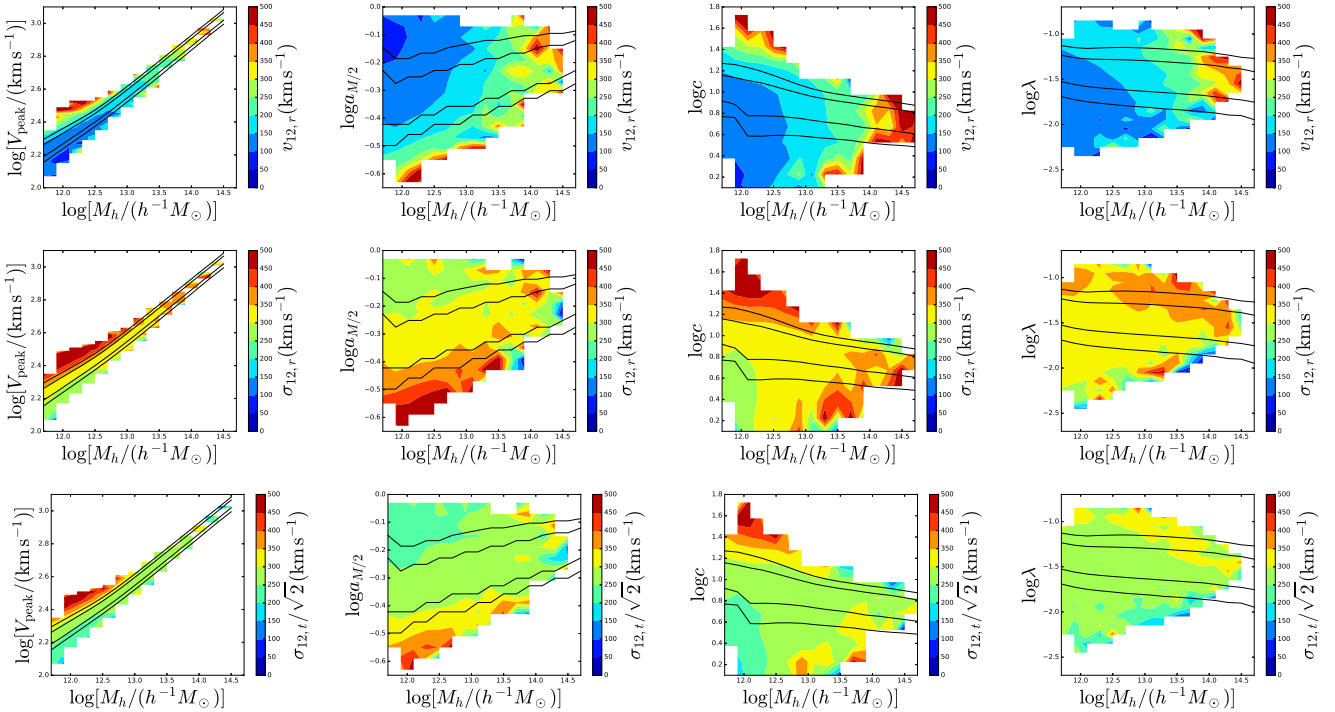


**Figure 11.** Dependence of halo pairwise velocity and velocity dispersions on halo mass and each of the assembly variables. Top, middle, and bottom panels show pairwise radial velocity, pairwise radial velocity dispersion, and pairwise transverse velocity dispersion, respectively. The pairwise velocity and velocity dispersions are evaluated at  $r \sim 10 h^{-1} \text{Mpc}$ . The four black curves in each panel mark the central 50 and 80 per cent of the distribution of the corresponding assembly variable as a function of halo mass.



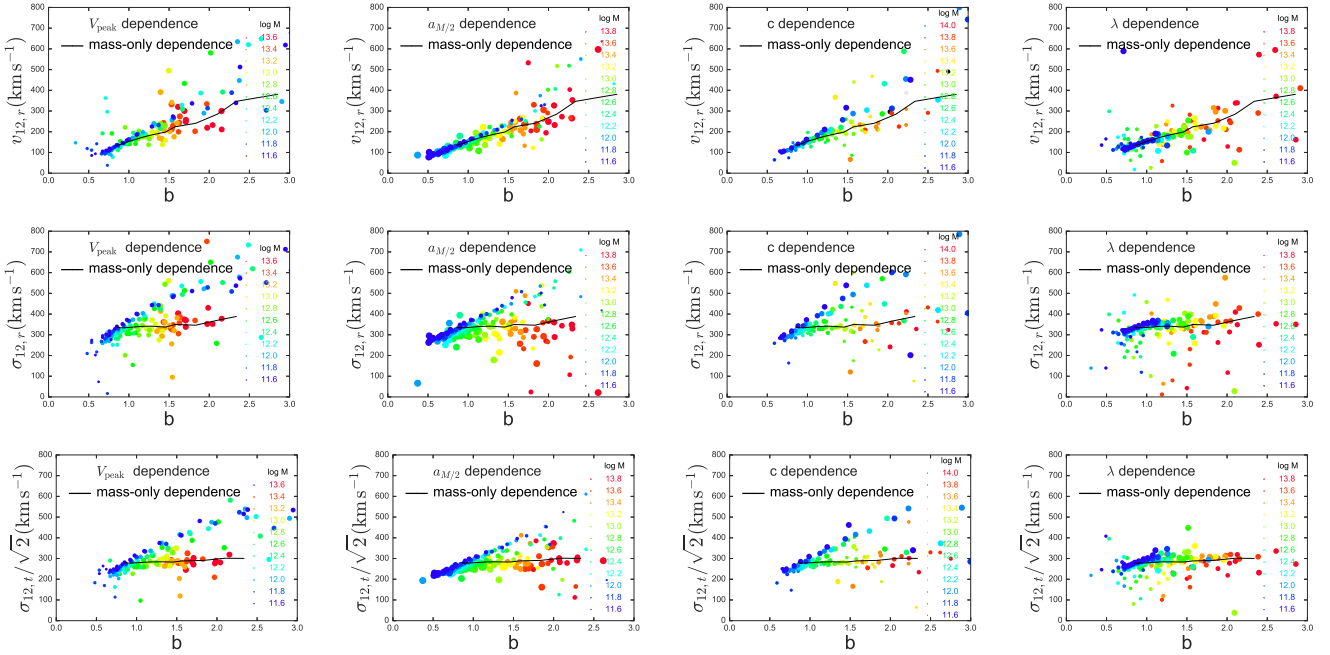


**Figure 12.** Relation between pairwise velocity and velocity dispersions and halo bias. Top, middle, and bottom panels show pairwise radial velocity, pairwise radial velocity dispersion, and pairwise transverse velocity dispersion versus halo bias, respectively. In each panel, the points are colour-coded by halo mass and their size indicates the value of the corresponding assembly variable. The pairwise velocity and velocity dispersions are evaluated at  $r \sim 10h^{-1}\text{Mpc}$ . The solid curve is computed from mass-only dependence of halo clustering.

the value of the bias factor in a way seen in Fig. 1. The plot is meant to show the  $v_{12,r}$ - $b$  sequence induced by assembly effect within each halo mass bin (represented by one colour) and as a collection from different mass bins.

In each panel, the curve is the relation derived from the dependence on halo mass only,  $v_{12,r}(M)$  versus  $b(M)$ , which is close to the expected linear relation. On average, the  $v_{12,r}$ - $b$  relation from the points tracks the curve quite well. At fixed mass, more strongly clustered haloes originated from assembly effect tends to have pairwise velocity shifted toward the curve (e.g. the blue points with the lowest mass). However, the magnitude of the shift is not large enough to make the points fall on top of the curve.

That is, within each halo mass bin, the  $v_{12,r}$ - $b$  relation from assembly effect shows deviations from the mass-only curve. In the  $v_{12,r}$ - $b$  relation as a whole from different mass bins, the assembly effect causes the scatter around the mass-only relation. The deviation and scatter from the expected  $v_{12,r}$ - $b$  relation implies that the environment plays a role more complicated than our naive expectation.

In the middle and bottom panels of Fig. 12, the pairwise radial and transverse velocity dispersions show a considerably large scatter around the mass-only curve. The mass-only curve is almost flat, which means that for haloes selected by mass the pairwise velocity dispersions are nearly independent of halo mass. Such a behaviour can be explained in linear theory by associating haloes with smoothed perturbation peaks (e.g. Bardeen et al. 1986; Sheth & Diaferio 2001). Once haloes are split by their assembly history, the pairwise velocity dispersions no longer follow the mass-only curve, especially for low mass haloes (blue points) from assembly effect almost monotonically increase with increas-

ing bias, substantially deviating from the mass-only curve. Low-mass haloes formed earlier (or with higher  $V_{\text{peak}}$  or higher concentration) can have 1D pairwise velocity dispersions as high as  $600\text{--}800\text{ km s}^{-1}$ , much higher than the mass-only value ( $\sim 300\text{ km s}^{-1}$ ). Interestingly they are even higher than those of massive haloes. This is consistent with those haloes being in denser environment, where larger pairwise velocity dispersions are expected (Sheth & Diaferio 2001). The other possible origin of the high velocity dispersion is that some low-mass haloes are stripped haloes ejected from massive haloes.

The above results indicate that assembly effect in the kinematics of haloes, in particular in the pairwise velocity dispersions, does not follow a simple description and that the environment can play an important role in shaping it.

As the assembly bias for low mass haloes is shown to be connected to their tidal environment (e.g. Hahn et al. 2009; Borzyszkowski et al. 2017; Paranjape et al. 2018), studying the dependence of pairwise velocity statistics on the tidal environment (e.g. characterised by the tidal tensor) would be a useful step to help understand the assembly effect on the halo kinematics.

The assembly effect on halo kinematics can affect the redshift-space clustering of haloes, raising the possibility of using redshift-space clustering to detect assembly effect with galaxy clustering. We analyse the redshift-space two-point correlation function and the multiple moments (monopole, quadrupole, and hexadecapole) of halo samples in mass and assembly variable bins. We find that the assembly effect on redshift-space clustering is mainly through the bias factor and that halo kinematics only introduce a minor effect. Similar to the scale-dependence case (§ 3.3), the halo assembly

effect may be hard to be revealed in practice from redshift-space clustering, but it deserves a further, detailed study.

## 5 SUMMARY AND DISCUSSION

Using dark matter haloes identified in the MultiDark MDR1 simulation, we investigate the joint dependence of halo bias on halo mass and halo assembly variables and the assembly effect on halo kinematics.

For the halo assembly variables (peak maximum circular velocity  $V_{\text{peak}}$ , halo formation scale factor  $a_{\text{M}/2}$ , halo concentration  $c$ , and halo spin  $\lambda$ ) considered in this work, the joint dependence of halo bias on halo mass and each assembly variable can be largely described as that halo bias increases outward from a point of global minimum in the plane of mass and assembly variable. All previous results of halo assembly bias measured for certain percentiles of a given halo assembly variable can be inferred from the above dependence and the distribution of assembly variable. We explore the possibility of finding an effective halo variable to minimise the assembly bias by using a combination of halo mass and spin. While an effective halo mass constructed through the combination absorbs the dependence of assembly bias on halo spin, at fixed effective mass, halo bias still depends on other assembly variables. The investigation indicates that assembly bias is multivariate in nature and that it is unlikely for one halo variable to absorb every aspect of the assembly effect.

From studying the joint dependence of halo bias on two assembly variables at fixed halo mass, we find that it is not necessarily true to predict the trend of assembly bias for one assembly variable solely based on that in the other assembly variable and their correlation. It only becomes possible if the gradient in halo bias follows the correlation direction. Whether the gradient and correlation directions align with each other relies on which two assembly variables to choose. It also depends on halo mass – with respect to the correlation direction, the gradient direction rotates as halo mass varies, showing the non-trivial nature of assembly bias.

We also study the kinematics of haloes under the assembly effect by dividing haloes according to halo mass and assembly variables. In general, more strongly clustered haloes have higher pairwise radial velocity and higher pairwise velocity dispersions. For low-mass haloes showing higher bias caused by assembly effect, the pairwise radial velocity tends to approach that of massive haloes of similar clustering amplitude, while the pairwise velocity dispersions can be substantially higher than those of the massive haloes. The results support the picture that the evolution of low mass haloes is influenced by the surrounding environment, especially the tidal field, and that some of low mass haloes could be ejected haloes around massive haloes. However, we do not find a simple description for the relation between halo kinematics and spatial clustering under assembly effect.

The assembly bias for low mass haloes ( $M_{\text{h}} \lesssim M_{\text{nl}}$ ) has a substantial scale dependence, showing as a drop on scales below  $\sim 3h^{-1}\text{Mpc}$ . The scale dependence of assembly bias and the assembly effect on halo kinematics can potentially provide an approach to identify assembly effects in galaxy clustering data through the shape of the scale-dependent galaxy bias and redshift-space distortions. However, the ef-

fect can be subtle, which can be masked by the one-halo term of galaxy clustering and the scatter between the galaxy properties and halo assembly. Further study is needed to see how and whether this approach works with high precision galaxy clustering data by incorporating the description of galaxy-halo connection with assembly effect included.

## ACKNOWLEDGEMENTS

We thank Kyle Dawson for useful discussions and the anonymous referee for constructive comments. The support and resources from the Center for High Performance Computing at the University of Utah are gratefully acknowledged. The CosmoSim database used in this paper is a service by the Leibniz-Institute for Astrophysics Potsdam (AIP). The MultiDark database was developed in cooperation with the Spanish MultiDark Consolider Project CSD2009-00064. The authors gratefully acknowledge the Gauss Centre for Supercomputing e.V. ([www.gauss-centre.eu](http://www.gauss-centre.eu)) and the Partnership for Advanced Supercomputing in Europe (PRACE, [www.prace-ri.eu](http://www.prace-ri.eu)) for funding the MultiDark simulation project by providing computing time on the GCS Supercomputer SuperMUC at Leibniz Supercomputing Centre (LRZ, [www.lrz.de](http://www.lrz.de)).

## REFERENCES

- Bardeen J. M., Bond J. R., Kaiser N., & Szalay A. S. 1986, *ApJ*, 304, 15
- Behroozi P. S., Wechsler R. H., & Wu H.-Y. 2013, *ApJ*, 762, 109
- Benson, A. J. 2017, *MNRAS*, 471, 2871
- Berlind A. A., & Weinberg D. H. 2002, *ApJ*, 575, 587
- Birnboim Y., & Dekel A. 2003, *MNRAS*, 345, 349
- Blake C., Kazin E. A., Beutler F., et al. 2011, *MNRAS*, 418, 1707
- Bond J. R., Cole S., Efstathiou G., & Kaiser N. 1991, *ApJ*, 379, 440
- Borzyszkowski, M., Porciani, C., Romano-Díaz, E., & Garaldi, E. 2017, *MNRAS*, 469, 594
- Busch P., & White S. D. M. 2017, *MNRAS*, 470, 4767
- Chaves-Montero J., Angulo R. E., Schaye J., et al. 2016, *MNRAS*, 460, 3100
- Colless M. 1999, *Philosophical Transactions of the Royal Society of London Series A*, 357, 105,
- Croft R. A. C., di Matteo T., Khandai N., et al. 2012, *MNRAS*, 425, 2766
- Dalal N., White M., Bond J. R., & Shirokov A. 2008, *ApJ*, 687, 12
- Dawson K. S., Kneib J.-P., Percival W. J., et al. 2016, *AJ*, 151, 44,
- Eisenstein D. J., Weinberg D. H., Agol E., et al. 2011, *AJ*, 142, 72,
- Faltenbacher A., & White S. D. M. 2010, *ApJ*, 708, 469
- Gao L., White S. D. M., Jenkins A., Stoehr F., & Springel V. 2004, *MNRAS*, 355, 819
- Gao L., Springel V., & White S. D. M. 2005, *MNRAS*, 363, L66
- Gao L., & White S. D. M. 2007, *MNRAS*, 377, L5
- Garaldi E., Romano-Díaz E., Borzyszkowski M., & Porciani C. 2018, *MNRAS*, 473, 2234
- Guo H., Li C., Zheng Z., et al. 2017, *ApJ*, 846, 61
- Hahn O., Carollo C. M., Porciani C., & Dekel A. 2007, *MNRAS*, 381, 41
- Hahn O., Porciani C., Dekel A., & Carollo C. M. 2009, *MNRAS*, 398, 1742

Han J., Li Y., Jing Y. P., Nishimichi T., Wang W., & Jiang C. 2018, arXiv:1802.09177

Harker G., Cole S., Helly J., Frenk C., & Jenkins A. 2006, MNRAS, 367, 1039

Hearin A. P. 2015, MNRAS, 451, L45

Jing Y. P. 1999, ApJ, 515, L45

Jing Y. P., Suto Y., & Mo H. J. 2007, ApJ, 657, 664

Kereš D., Katz N., Weinberg D. H., & Davé R. 2005, MNRAS, 363, 2

Klypin A. A., Trujillo-Gomez S., & Primack J. 2011, ApJ, 740, 102

Lazeyras T., Musso M., & Schmidt F. 2017, J. Cosmology Astropart. Phys., 3, 059

Lin Y.-T., Mandelbaum R., Huang Y.-H., et al. 2016, ApJ, 819, 119

Macciò A. V., Dutton A. A., van den Bosch F. C., et al. 2007, MNRAS, 378, 55

Mao Y.-Y., Zentner A. R., & Wechsler R. H. 2018, MNRAS, 474, 5143

McEwen J. E., & Weinberg D. H. 2016, arXiv:1601.02693

Miyatake H., More, S., Takada M., et al. 2016, Physical Review Letters, 116, 041301

Mo H. J., & White S. D. M. 1996, MNRAS, 282, 347

Paranjape A., & Padmanabhan N. 2017, MNRAS, 468, 2984

Paranjape A., Hahn O., & Sheth R. K. 2018, MNRAS, 476, 3631

Prada F., Klypin A. A., Cuesta A. J., Betancort-Rijo J. E., & Primack J. 2012, MNRAS, 423, 3018

Press W. H., & Schechter P. 1974, ApJ, 187, 425

Salcedo A. N., Maller A. H., Berlind A. A., et al. 2018, MNRAS, 475, 4411

Sheth R. K., Diaferio A., Hui L., & Scoccimarro R. 2001, MNRAS, 326, 463

Sheth R. K., & Diaferio A. 2001, MNRAS, 322, 901

Shi J., Wang H., & Mo H. J. 2015, ApJ, 807, 37

Sunayama T., Hearin A. P., Padmanabhan N., & Leauthaud A. 2016, MNRAS, 458, 1510

Tinker J., Kravtsov A. V., Klypin A., et al. 2008, ApJ, 688, 709-728

Trenti, M., Smith, B. D., Hallman, E. J., Skillman, S. W., & Shull, J. M. 2010, ApJ, 711, 1198

Wang H., Mo H. J., & Jing Y. P. 2009, MNRAS, 396, 2249

Wang H., Mo H. J., Jing Y. P., Yang X., & Wang Y. 2011, MNRAS, 413, 1973

Wechsler R. H., Bullock J. S., Primack J. R., Kravtsov A. V., & Dekel A. 2002, ApJ, 568, 52

Wechsler R. H., Zentner A. R., Bullock J. S., Kravtsov A. V., & Allgood B. 2006, ApJ, 652, 71

Wetzel A. R., Tinker J. L., Conroy C., & van den Bosch F. C. 2014, MNRAS, 439, 2687

White S. D. M., & Rees M. J. 1978, MNRAS, 183, 341

Yang X., Mo H. J., & van den Bosch F. C. 2003, MNRAS, 339, 1057

York D. G., Adelman J., Anderson J. E., Jr., et al. 2000, AJ, 120, 1579,

Zehavi I., Zheng Z., Weinberg D. H., et al. 2005, ApJ, 630, 1

Zehavi I., Zheng Z., Weinberg D. H., et al. 2011, ApJ, 736, 59

Zentner A. R., Hearin A. P., & van den Bosch F. C. 2014, MNRAS, 443, 3044,

Zentner A. R., Hearin A., van den Bosch F. C., Lange J. U., & Villarreal A. 2016, arXiv:1606.07817,

Zhang H.-Y., & Jing Y.-P. 2004, Chinese J. Astron. Astrophys., 4, 507

Zheng Z., Tinker J. L., Weinberg D. H., & Berlind A. A. 2002, ApJ, 575, 617

Zheng Z., Berlind A. A., Weinberg D. H., et al. 2005, ApJ, 633, 791

Zhu G., Zheng Z., Lin W. P., et al. 2006, ApJ, 639, L5

Zu Y., Mandelbaum R., Simet M., Rozo E., & Rykoff E. S. 2017, MNRAS, 470, 551

## APPENDIX A: MASS RESOLUTION EFFECT ON HALO BIAS AND PAIRWISE VELOCITY STATISTICS

In the main analysis in this paper, we primarily use haloes from the MDR1 simulation, which has particle mass of  $8.721 \times 10^9 h^{-1} M_\odot$ . Paranjape & Padmanabhan (2017) show that for haloes with less than 400 particles, halo concentration may not be determined accurately, usually lower than the true value (their Fig.2; also see Fig.9 of Trenti et al. 2010). The distribution of other assembly variables (such as spin) for haloes of low number of particles can also be affected (e.g. Fig.9 in Trenti et al. 2010 and Fig.3 in Benson 2017). Such a numerical effect would potentially affect the pattern of the dependence of halo bias and velocity statistics on assembly variables for halos of mass below  $3.5 \times 10^{12} h^{-1} M_\odot$  in the MDR1 simulation. To test the effect, we make use of the Bolshoi simulation, with the same cosmology but a 64 times higher mass resolution. The mass of haloes with 400 particles in the Bolshoi simulation is  $5.5 \times 10^{10} h^{-1} M_\odot$ , well below the minimum mass in our analysis.

First, we perform similar calculations as in Fig. 1, but using haloes in the Bolshoi simulation for  $\log[M_h/(h^{-1} M_\odot)] < 12.8$ . The results are presented in Fig. A1. By comparing with those in Fig. 1, we see that the trend in the joint dependence of halo bias on halo mass and one assembly variable from the Bolshoi simulation is similar to that from the MDR1 simulation in the mass range considered in the paper. The test assures that we can present the main results based on MDR1 simulation. The large volume of MDR1 compared to Bolshoi has the advantage of making the halo bias calculation less noisy and enabling the inclusion of a larger range in assembly variable at fixed mass, which is clearly seen when comparing Fig. 1 and Fig. A1. For the above reason, the results on bias (except for those in Section 3.2, see below) from the MDR1 simulation are shown in the paper. We caution, however, that for investigations or applications that require accurate values of halo bias, the mass resolution effect needs to be accounted for.

For the investigation with effective halo mass in Section 3.2, we need to combine the Bolshoi and MDR1 simulation. This is not mainly driven by the above numerical effect, but the need for low mass haloes. As can be seen from the left panel of Fig. 2, for effective halo mass in the range  $\log[M_{\text{eff}}/(h^{-1} M_\odot)] \sim 11-12.5$ , we need to reach haloes with high spin and low mass (below  $\log[M_h/(h^{-1} M_\odot)] \sim 11.6$ ), which are covered incompletely in the MDR1 simulation. A combination of MDR1 and Bolshoi is therefore necessary for the effective mass analysis (see Section 3.2 for details).

Then we analyse the pairwise velocity statistics of haloes of  $\log[M_h/(h^{-1} M_\odot)] \sim 11.73$  in the Bolshoi simulation. Fig. A2 shows the dependence of pairwise velocity and velocity dispersion on assembly variable, which is to be compared to Fig. 10 with the MDR1 simulation. For the cases with  $V_{\text{peak}}$ ,  $a_{M/2}$ , and  $c$  (the left three columns), the trends from the Bolshoi simulation well track those from the MDR1 simulation. There are slight amplitude shifts for

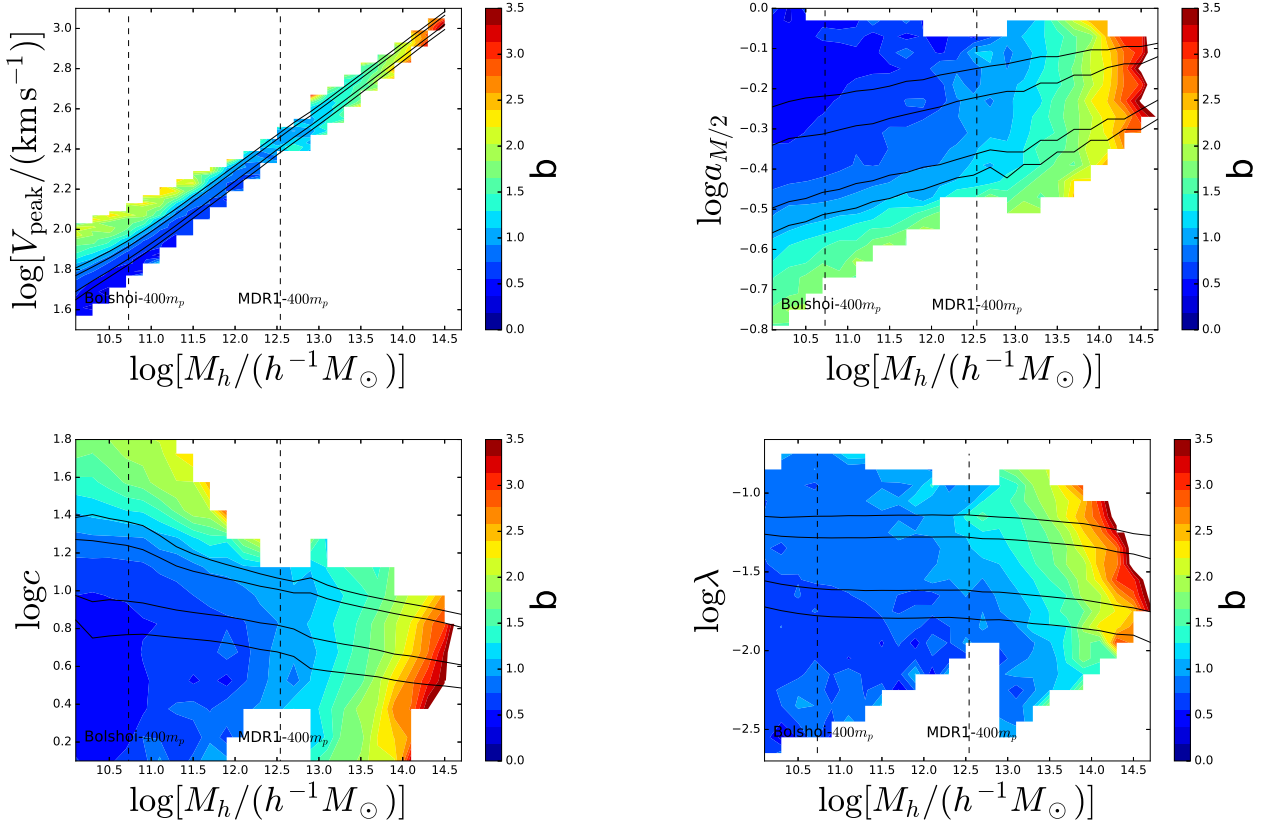


**Figure A1.** Same as Fig. 1, but the Bolshoi simulation is used for  $\log[M_h/(h^{-1}M_\odot)] < 12.8$  and MDR1 simulation for higher mass. The two vertical dashed lines in the each panel indicate the masses of haloes with 400 particles in the two simulations.

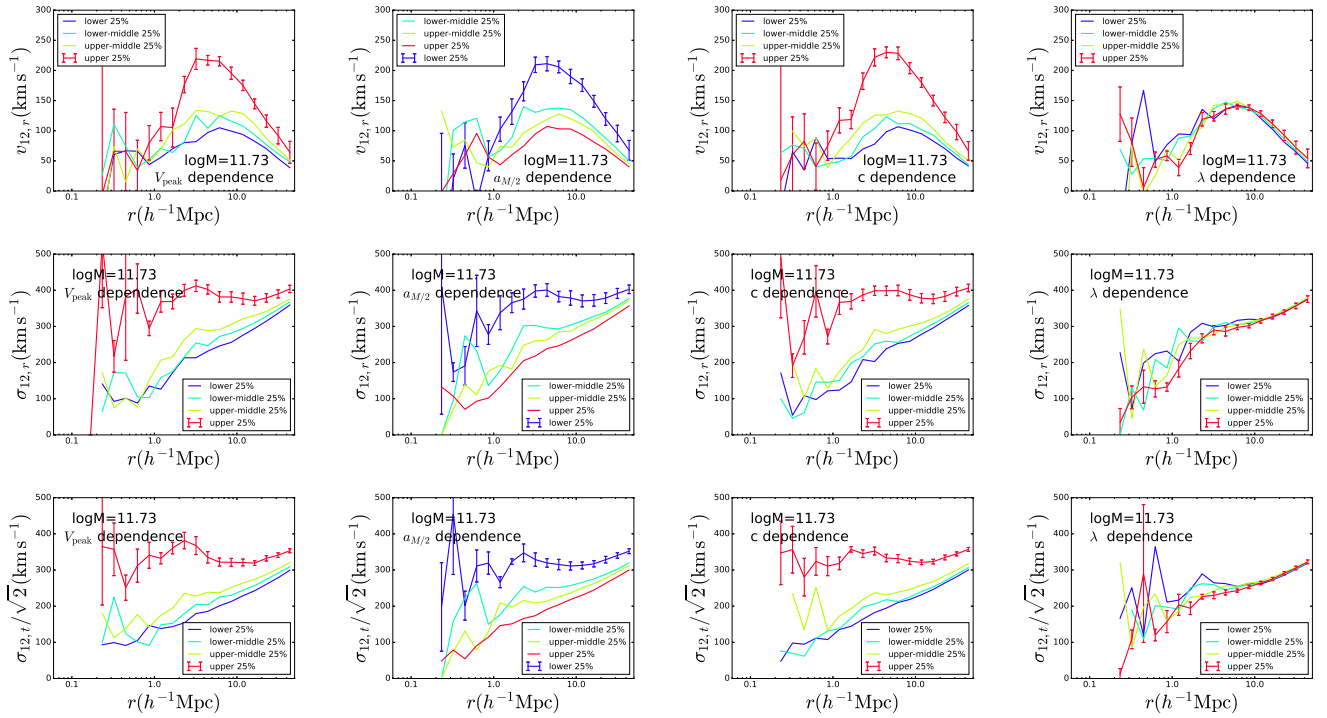


**Figure A2.** Same as Fig. 10, but haloes from the Bolshoi simulation is used for the analysis.



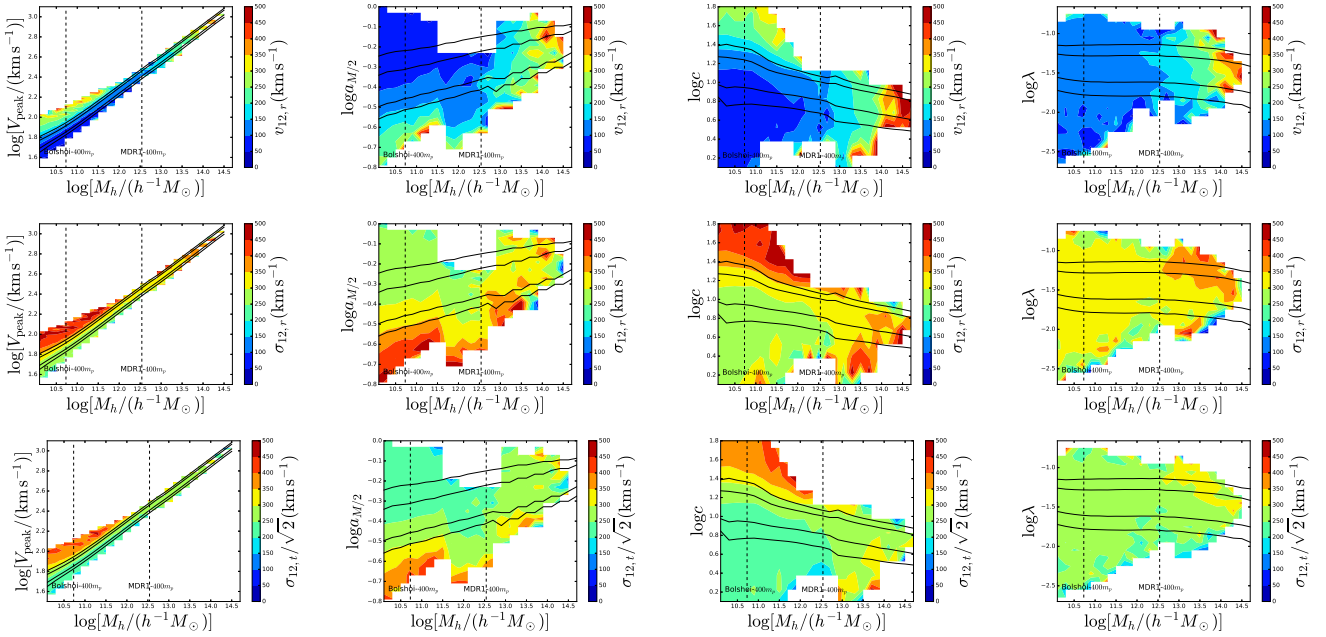


**Figure A3.** Same as Fig. 11, but the Bolshoi simulation is used for  $\log[M_h/(h^{-1}M_\odot)] < 12.8$  and MDR1 simulation for higher mass. The two vertical dashed lines in the each panel indicate the masses of haloes with 400 particles in the two simulations.

the corresponding curves from the two simulations, which can be partly explained by the sample variance effect (i.e. difference in the long-wave length modes in the two simulations). The mass resolution may also contribute. Imagine that we have a simulation with the same box size and initial condition as Bolshoi but with MDR1 mass resolution. For Bolshoi haloes of a given concentration, those of the corresponding MDR1-resolution haloes would have a scatter (e.g. [Paranjape & Padmanabhan 2017](#); [Trenti et al. 2010](#)). That is, for the same percentile, haloes from the two simulations would not have the exact correspondence, and the pairwise velocity amplitude is expected to be slightly different. For the above three assembly variables, the pattern of the dependence of pairwise velocity statistics on the value of assembly bias from the Bolshoi simulation is similar to that from the MDR1 simulation, as can be seen by comparing Fig. A3 and Fig. 11.

For the case with halo spin  $\lambda$ , the pairwise velocity statistics from the percentile analysis seem to be different between the MDR1 and Bolshoi simulations (right panels of Fig. 10 and Fig. A2). With the MDR1 simulation, there is a clear trend of higher pairwise velocity and velocity dispersion for haloes of higher spin, although it is substantially weaker than those with other three assembly variables. With the Bolshoi simulation, however, we do not see such a clear trend (also see the corresponding panels of Fig. A3). If what Bolshoi suggests is close to the truth, given the expected scatter in determining the spin parameter for a low-resolution simulation (e.g. [Trenti et al. 2010](#); [Benson 2017](#)), we would not expect to see any trend with the MDR1 simulation. However, here we have the opposite results. We note that the error bars with the Bolshoi simulation analyses are substantially larger than those with the MDR1. It is possible that the sample variance effect in the Bolshoi simulation masks the spin dependence, i.e. the noise level is too high to re-

veal the intrinsically weak trend. The other possibility is that with low-resolution simulations the spin measurement is more easily affected by environment and hence halo assembly, making the scatter mentioned above not random. Further investigations using simulations of the same initial condition and different resolutions, like those in [Trenti et al. \(2010\)](#), would help resolve the issue of the spin-dependence of the pairwise velocity statistics.

To summarise, from comparing the halo statistics with MDR1 and Bolshoi simulations, for most results presented in this paper, the MDR1 simulation works well in revealing the patterns related to assembly variables, which has the benefit of better statistics from the much larger volume. For the effective halo mass analysis, we have to include the Bolshoi simulation to reach haloes of much lower mass for completeness consideration. For halo pairwise velocity statistics, the spin case appears to be different between the two simulations, weak trend with the MDR1 simulation and the lack of trend with the Bolshoi simulation. The cause of the apparent discrepancy is not entirely clear, which could be noise in the Bolshoi simulation or some unknown environment-dependent systematic effect in halo spin measurement. In the main text, we choose to present the spin results from the MDR1 simulation, but put the caveat that there is an apparent difference compared to those from the Bolshoi simulation.

This paper has been typeset from a  $\text{\LaTeX}$  file prepared by the author.